university of groningen / faculty of science and engineering / mathematics and applied mathematics

Minimize Propellant Slosh During Moon Landing

Bachelor's Project Mathematics

May 2024

Student: Maarten Hamming

First supervisor: Dr. ir. R. Luppes

Second assessor: Dr. A. E. Sterk

Abstract

This research delves into the intricate dynamics of propellant sloshing during spacecraft lunar landing manoeuvres, aiming to minimize its effects through various approaches. Using the ComFLOW software, the study examines the impact of different fuel tank shapes, fuel types, and landing manoeuvre strategies. Investigation through comparing cylindrical and spherical fuel containers shows negligible differences, but the ellipsoidal design exhibits reduced slosh-induced forces. The research also explores the effects of using different propellant types with varying physical properties. Lower density fuels, such as liquid hydrogen, results in lower average and peak forces compared to denser fluids like RP-1, and ethanol. Additionally, alternative landing maneuver strategies are evaluated, focusing on timing and coordination. Simultaneous rotation and deceleration with extended rotation duration shows promise in minimizing slosh-induced disturbances. The findings underscore the importance of fuel tank design, fuel type selection, and maneuver coordination in optimizing spacecraft stability during critical landing phases.

Contents

1 Introduction **3**

2 Research Question **4**
2.1 Method 4

3 Numerical Model **5**
3.1 Navier-Stokes equations 5
3.2 Discretization 5
3.3 Force Box 7
3.4 Grid Conversion Study 8

4 Manoeuvre **9**
4.1 Dominant Forces 11

5 Effect of Tank Geometry on Propellant Slosh **12**
5.1 Parameters 12
5.2 Results 13
5.3 Observations 18

6 Effect of Fuel Type on Propellant Slosh **19**
6.1 Parameters 19
6.2 Results 19
6.3 Observations 24

7 Changing the landing manoeuvre **25**
7.1 Results 25
7.2 Observations 29

8 Conclusion **30**
8.1 Discussion 31

9 Appendix A: Grid conversion study results **33**

1 Introduction

Since the historic landing of Apollo 11 on the surface of the moon in 1969, human fascination with space exploration has only increased. In more modern times, technological advancements have brought us closer to realizing ambitious missions, including the colonization of Mars.

Central to the success of these ventures is the reliable and precise landing of spacecraft on planets and moons, a task that comes with challenges, among which is the unpredictability of propellant slosh in fuel tanks. The sloshing phenomenon, characterized by the movement of liquid propellant within spacecraft fuel tanks during flight and descent, has long been recognized as a significant factor in spacecraft stability and control. During the Apollo missions, engineers struggled with disturbances induced by propellant slosh causing the Apollo 11 to lose control and require manual piloting.

With the emergence of private space exploration companies like SpaceX and the renewed focus on space exploration, the need for more sophisticated approaches to minimize sloshing has become increasingly apparent. This research seeks to explore the impact of sloshing in spacecraft fuel tanks, with a specific focus on a spacecraft landing on the moon. By simulating real world manoeuvres the aim is to identify strategies for effectively minimizing slosh-induced disturbances during lunar landings. Central to this investigation is an understanding of the forces governing propellant slosh. The interaction between the spacecraft's movement and the sloshing fuel generates complex interactions, giving rise to forces acting on the tank and can induce oscillations, instabilities, and even unexpected torques on the spacecraft, leading to a significant risk to mission success.

ComFLOW is a powerful computational tool used to model and analyze fluid flow phenomena in various engineering and scientific applications. With this tool the aim is to develop strategies to reduce interference caused by propellant slosh in lunar landers. These strategies include new tank designs, fuel methods or even introducing different manoeuvres. This research endeavor attempts to aid the advancement of space exploration by addressing a critical, yet often overlooked, aspect of spacecraft design and operation. The minimization of the impact of propellant slosh on lunar landers is sought to improve their reliability, stability, and safety, ultimately paving the way for humanity's continued exploration of the cosmos, from the Moon to Mars and beyond.

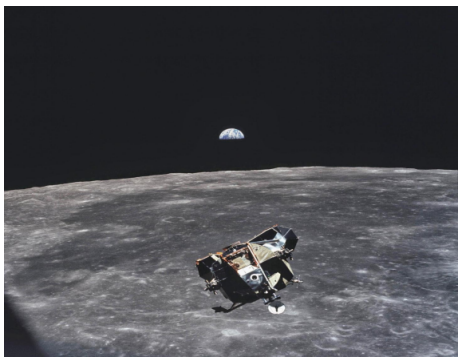

Figure 1: Apollo 11 lunar lander approaching the moon[1]

2 Research Question

This research will try to analyze the effects of propellant slosh during a landing manoeuvre on the moon with differently shaped fuel tanks, multiple fuel types and two new landing trajectories and attempts to minimize this effect. History has told us that these effects should not be underestimated and with the current interest in space travel, especially reusable rockets, the research done on sloshing in multiple scenarios can be beneficial. To simulate real world examples the use of ComFLOW software is prevalent throughout the process of examining the differences with various parameters. As such the research question of this article is as follows:

How can the force generated by slosh in the fuel container of a spacecraft be minimized while performing a landing manoeuvre on the moon.

2.1 Method

This research is a direct continuation of Raphael Ashruf's research done in 2020.[2] Ashruf used ComFLOW to better understand the effects of sloshing during certain manoeuvres in space. He performed various simulations including several manoeuvres with cylindrical fuel tanks filled to different percentages and moving over time frames of different length. The main conclusion of these simulations was that if the spacecraft takes twice as long to perform the manoeuvre, the force effects of sloshing on the spacecraft are roughly halved. [2]

Studies on ComFLOW have to be performed to validate the correctness (of implementation) of the software. This includes simpler examples and recreating Ashruf's simulations. In order to answer the research question, after understanding the software a few different scenarios will be explored.

- Adaptation of the geometry of the fuel tank.
- Several fuel types with distinct physical properties.
- Modification of the landing manoeuvre.

3 Numerical Model

3.1 Navier-Stokes equations

This research involves using the ComFLOW software to simulate fluid flow. ComFLOW is extensively utilized in offshore engineering projects for its capability to model intricate fluid dynamics in marine environments. Engineers and researchers rely on ComFLOW to simulate various hydrodynamic phenomena, including wave interactions, fluid behavior around offshore structures such as platforms and vessels, and the influence of currents on marine installations. Its application enables evaluation of offshore systems' performance, aiding in risk assessment and safety enhancement measures. Furthermore, ComFLOW provides invaluable insights into flow patterns, which are crucial for optimizing resource allocation, planning maintenance activities, and conducting environmental impact assessments in offshore projects.

To this end, ComFLOW uses the Navier-Stokes equations for incompressible (constant density) and isothermal (constant temperature) flow. These equations describe the conservation of mass in equation (1) and momentum in equation (2) and require boundary conditions at a certain boundary $d\Omega$ of the domain Ω over which the equations are defined. Solid boundaries need to be impenetrable by the fluid. Moreover, the fluid needs to 'stick' to the boundary due to viscosity. The Navier-Stokes equations for incompressible flow are:

$$\nabla \cdot \mathbf{u} = 0. \tag{1}$$

$$\frac{\partial \mathbf{u}}{\partial t} + (\mathbf{u} \cdot \nabla)\mathbf{u} = -\frac{1}{\rho}\nabla p + \frac{\mu}{\rho}\nabla \mathbf{u} + \mathbf{F}. \tag{2}$$

Where $\mathbf{u} = (u, v, w)$ is the velocity vector, p is the pressure, μ is the dynamic viscosity, ρ is the density and $\mathbf{F}$ are external forces induced by the tank by e.g. deceleration of the spacecraft and gravity.[3] Equation (1), relating to the conservation of mass principle, states that the rate of change of mass within a control volume must equal the net mass flux, i.e. the in and outflow across its boundaries.[4] For incompressible flow, density remains constant, resulting in the divergence of the velocity field being zero. The conservation of momentum (2 is derived by considering the forces acting on a fluid element in both the temporal and spatial domains. Applying Newton's second law to each direction yields the Navier-Stokes equations, which describe the evolution of the velocity field over time.

3.2 Discretization

The Navier-Stokes equations are not solvable analytically and thus a discretization is established to numerically solve them. This is done by creating a rectangular Cartesian grid that fully covers the real fluid domain Ω. The grid is created with cell labeling as shown in Figure 2. Initially three types of cells are labeled to distinguish between boundary (**B**), exterior (**X**) and fluid. The fluid cells are then divided into three categories as well: empty (**E**), surface (**S**) or fluid (**F**).[3]

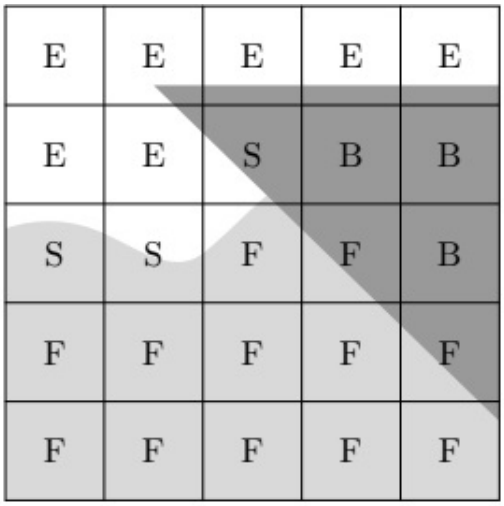

Figure 2: Cell labeling of a ship in a body of fluid (empty (**E**), surface (**S**) or fluid (**F**)) [3]

To solve the Navier-Stokes equations on the Cartesian grid, the equations need to be discretized in time and space. The time discretization is done in ComFLOW by choosing to use either the Forward Euler method or the Adams-Bashforth method.[3] The Forward Euler method for a given initial value problem

$$\frac{dy}{dt} = f(t,y), y(0) = y_0$$

is finding y_{n+1} after every time step h using the iteration

$$y_{n+1} = y_n + hf(t_n, y_n).$$

This is an explicit first order one-step method. The Adams-Bashforth method is a multi-step method and for the initial value problem stated above it reads

$$y_{n+2} = y_{n+1} + \frac{3}{2}hf(t_{n+1}, y_{n+1}) - \frac{1}{2}hf(t_n, y_n)$$

and is a second order explicit method. These two methods differ in accuracy, stability and computational complexity. Forward Euler is a first-order method, which means that as the step size h decreases, the error decreases linearly. The method can also be unstable for ordinary differential equations where the step size is too large relative to the dynamics of the problem, which can in the worst case lead to divergence. The forward Euler method is relatively simple in computation, since it only requires the calculation of a derivative at the current time step. The second order Adams-Bashforth method, on the other hand, is a multi-step method that can achieve higher accuracy. The Adams-Bashforth method used in ComFLOW is second-order, providing better accuracy compared to the Forward Euler method for the same step size. However, Adams-Bashforth is generally less stable and requires smaller time-steps to ensure stability. Though there are definitely benefits to using Adams-Bashforth, the increase in computation time is reason enough to use the less accurate but faster forward Euler method in this research.

To discretize the Navier-Stokes equations in space there are again options in ComFLOW, based on the finite volume method. The options are (second-order) central discretization and first or second order upwind discretization. First order upwind discretization is chosen for the simulations in this research, which has the advantage of being more stable.[3] Unfortunately this

discretization can bring forth an issue called numerical viscosity, which means that during the simulation this discretization might make the fluid appear more viscous than in reality. The effect of numerical viscosity for similar simulations has been tested in 2020 and no significant numerical viscosity problems arose.[2]

ComFLOW employs dynamic time steps, allowing the time steps (denoted as δt) to fluctuate during a simulation. This adjustment is determined by the CFL stability condition. The CFL number dictates whether the time step should be decreased for accuracy and stability or increased to save computation time.

$$CFL = \max_{i,j,k}\left(\frac{\left|u_{ijk}\delta t\right|}{h_{x,i}} + \frac{\left|v_{ijk}\delta t\right|}{h_{y,i}}\right) + \frac{\left|w_{ijk}\delta t\right|}{h_{z,i}}, \tag{3}$$

where u, v and w are velocity components and h_x, h_y and h_z denote grid sizes in the respective directions. A maximum time step (δt_{max}), a minimum CFL number (CFL_{min}), and a maximum CFL number (CFL_{max}) can be set in the initial configuration. If the computed CFL number exceeds CFL_{max}, the time step is halved to achieve accuracy. Conversely, if the computed CFL number remains below CFL_{min} for ten consecutive time steps, the time step is doubled to reduce computation time. However, the time step is not doubled if doing so would exceed δt_{max}, even if the computed CFL number falls below CFL_{min}.[3]

3.3 Force Box

To calculate the forces on the spacecraft induced by the liquid fuel, a force box is created in the simulation. A force box finds the force in all three orientations (x,y,z) in closed cells and does this by calculating the integral of the pressure p multiplied by the unit normal vector $\mathbf{n}$ to the boundary surface S.

$$\mathbf{F} = \int_S p\mathbf{n}dS \tag{4}$$

The calculated forces are stored by ComFLOW in a table. Through the post processing unit graphs can be created to get an insight in the evolution of these forces. To calculate the total force on the tank, a force box is created around the entire tank. The size of this force box therefore needs to be at least of the size of the spacecraft, such that ComFLOW can calculate the total force applied to the spacecraft. For this a force box with x,y and z ranging from -100 to 100 will suffice, but any values greater than the geometry described by the spacecraft would be adequate. The entire spacecraft (cylinder) with the force box around it is shown in Figure 3. The forces are calculated several times during the simulation, which for the compared cases is 120 times. A graph of the forces is then created to visualize the development of the forces during the manoeuvre. [3]

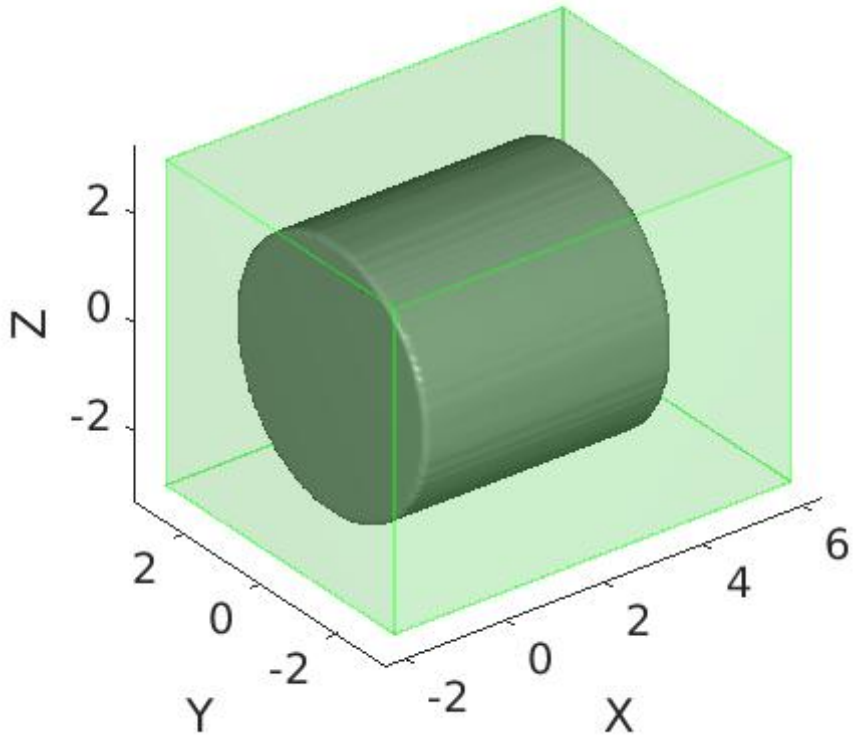

Figure 3: Cylindrical spacecraft entirely covered by a force box (green)

3.4 Grid Conversion Study

The initial grid consists of 80x80x80 such that the total number of cells equals 512000. To ensure that the grid is fine enough and the results are valid, a grid conversion study needed to be done. This examination of convergence in a computational fluid dynamics (CFD) simulation is a necessary approach for assessing the discretization error. This involves conducting simulations on a more refined grid, in this case 120x120x120 leading to approximately 1.7 million cells. In appendix A the comparison of the two simulations is shown and minimal difference is observed, such that it is ensured that the constructed grid of 512000 cells is adequate.

4 Manoeuvre

The focus of this research lies on the landing operation of a spacecraft when it is already close to the surface of the moon. Assumed is that the spacecraft approaches the moon at a velocity of 27.8 m/s where the fuel tank horizontally aligns with the the moon as in point A in Figure 4. The trajectory displayed will stay the same throughout the research, the time frame of rotation and deceleration will change in Section 7 and this is further explained there.

For now, consider two processes during the manoeuvre. A deceleration of the spacecraft to 1 m/s, this happens over the X-axis. The second process is the turning of the spacecraft 90 degrees such that the bottom (landing gear) is aligned with the surface of the moon. To apply these motions to the fuel tank, ComFLOW requires input files with complete distance, velocity and acceleration values for each time-step during the whole landing procedure. The complete manoeuvre lasts 35 seconds with time-steps of 0.1 seconds. For the shape and fuel simulations, studied in Sections 5 and 6 the deceleration happens during the first 25 seconds, from A to C, and the turning process during the last ten seconds, from C to D. The turning process is also divided in an accelerating rotation in the first half and decelerating rotation in the last five seconds. The specific values are calculated by the equations of motion for the rotation and horizontal surge of the spacecraft. With $x(t)$ and its derivatives denoting the horizontal displacement, velocity and acceleration on the time frame $t = 0s$ to $t = 25s$ and $\omega(t)$ and its derivatives denoting the rotational displacement, velocity and acceleration on the time frame $t = 25$ to $t = 35s$, the equations can be summarized as

$$x(t) = \begin{cases} 27.8 * t - \frac{at^2}{2}, & t \in [0,25] \\ x(25) + 1 * (t-25), & t \in (25,35] \end{cases} \tag{5a}$$

$$\dot{x}(t) = \begin{cases} 27.8 - a * t, & t \in [0,25] \\ 1, & t \in [25,35] \end{cases} \tag{5b}$$

$$\ddot{x}(t) = \begin{cases} -a, & t \in [0,25] \\ 0, & t \in [25,35] \end{cases} \tag{5c}$$

$$\omega(t) = \begin{cases} -\frac{\alpha(t-25^2)}{2}, & t \in [25,30] \\ -(10 * \alpha * (t-25) - \frac{\alpha(t-25)^2}{2} - \frac{\pi}{2}), & t \in [30,35] \end{cases} \tag{6a}$$

$$\dot{\omega}(t) = \begin{cases} \alpha * (t-25), & t \in [25,30] \\ -(10\alpha - (t-25)\alpha), & t \in [30,35] \end{cases} \tag{6b}$$

$$\ddot{\omega}(t) = \begin{cases} \alpha, & t \in [25,30] \\ -\alpha, & t \in [30,35] \end{cases} \tag{6c}$$

Where a is the acceleration in the horizontal surge motion calculated as

$$a = \frac{\Delta v}{t_C - t_A} = \frac{26.8 m/s}{25s}$$

and α is the rotational acceleration for a 90 degree or $\frac{\pi}{2}$ turn calculated as

$$\alpha = \frac{\pi}{2(\frac{t_D - T_C}{2})^2} = \frac{\pi m/s}{50s}.$$

The values for the sway, heave, jaw and roll (see Figure 4) will remain zero throughout the research.[2]

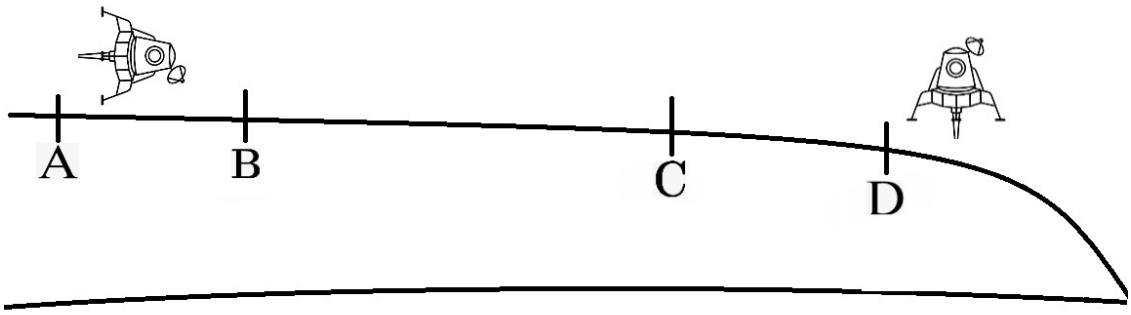

Figure 4: Trajectory of a lunar lander close to the surface of the moon

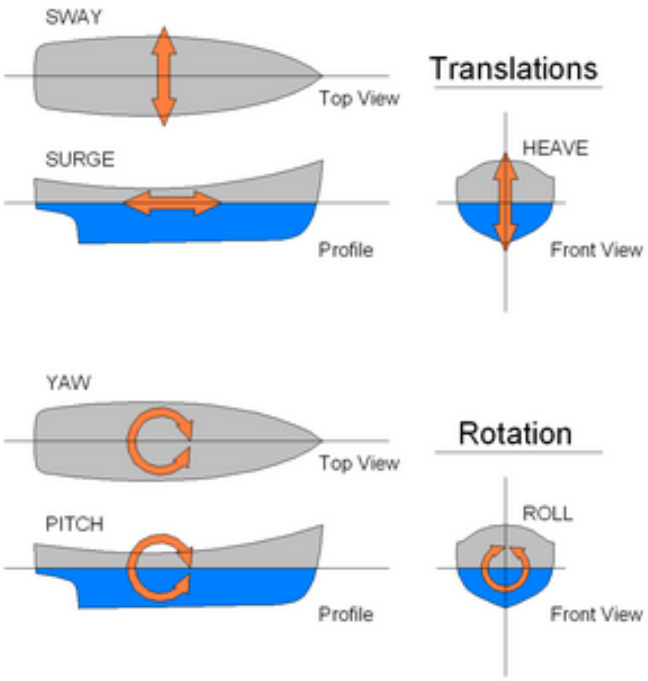

Figure 5: Ship translational and rotational motions[5]

4.1 Dominant Forces

The deceleration encountered induces a force upon the fluid within the spacecraft, compelling it towards the right side of the interior wall, given the spacecrafts rightward motion. As explained before, this motion has a deceleration of $a = \frac{\Delta v}{\Delta t} = \frac{27.8-1}{25} m/s^2$ over 25 seconds and as such a straightforward calculation gives the force in the direction of the x-axis. The base case tank, filled 50% has dimensions such that the volume of the liquid inside is $\frac{1}{2}\pi * 4 * \frac{8}{3} = \frac{16\pi}{3} m^3$ and using the density of water at 20° Celsius, this leads to the following force associated with deceleration.

$$F_x = m * a = \frac{16\pi m^3}{3} * 10^3 kg/m^3 * \frac{27.8-1}{25} m/s^2 \approx 1.8 * 10^4 N. \tag{7}$$

The other force acting on the spacecraft is the gravitational force acting on the z- axis, which for a surface gravity of the moon at $1.62 m/s^2$ is easily found by computing

$$F_z = m * g_{moon} = \frac{16\pi m^3}{3} * 10^3 kg/m^3 * -1.62 m/s^2 \approx -2.7 * 10^4 N. \tag{8}$$

Note that although the values are of similar magnitude as the values presented by Ashruf [2], in order to be able to adapt the volume easily and accurately for the next section, these changes in size were made. This does not impact the reliability of the results since all calculations are affected equally and the effects of propellant slosh are measured by the deviations from these main forces stated in equations (7) and (8).

5 Effect of Tank Geometry on Propellant Slosh

One of the first changes that come to mind when trying to minimize the effect of propellant slosh in a spacecraft is to smooth-out the fuel container of the spacecraft. This section will focus on simulations done in ComFlow using three different shapes of fuel containers. The three shapes tested in this section are cylinder, ellipsoid and sphere. These shapes are chosen for the following reasons. A cylinder has already thoroughly been tested by Ashruf in his research [2] and is used as the base case here. In his research sloshing was eminent and had a recorded impact on the overall force applied to the vehicle. As a comparison, the first simulation is a repetition of Ashruf's simulation done with a cylindrical fuel tank filled to 50% [2], following the movement described in Section 4. Since a smoother surface of container is expected to reduce the force generated by slosh, as this has been shown in studies done for fuel tanks on earth[6], an ellipsoid and ultimately a sphere are chosen to be compared to the cylinder.

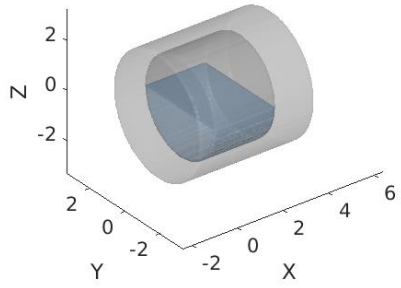

(a) Cylindrical fuel tank

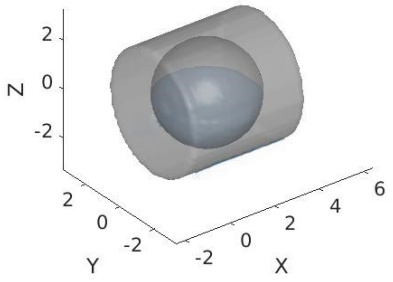

(b) Spherical fuel tank

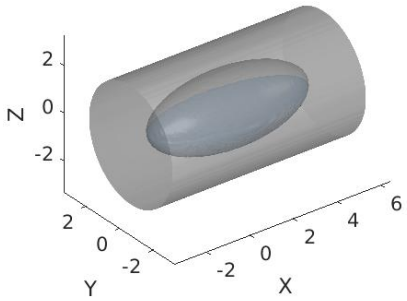

(c) Ellipsoidal fuel tank

Figure 6: Starting positions of the differently shaped fuel tanks inside a cylindrical spacecraft

5.1 Parameters

The defined geometry of the fuel tank used for the simulations is the most notable change in this section. The global shape of the spacecraft is a cylinder that fully envelops the fuel tank, this cylinder will stay the same for all three simulations. What does change, however, is the shape of the fuel tank inside the spacecraft. In Figures 6a, 6b and 6c the spacecraft with cylindrical fuel tank inside the full body of the spacecraft is displayed. In order to find noteworthy results the same amount of fuel will be used throughout the three simulations. This is obtained by simulating the fuel tanks with the same volume ($V \approx \frac{16\pi}{3}$), the dimensions stated for the three

shapes are listed in table 1. Note that since the fuel tank is filled to 50% the volume of the body of fuel is exactly half of the volume of the entire tank.

	Length (x-axis)	Radius (y/z-axis)
Entire spacecraft	5	$5/2$
Cylindrical tank	$8/3$	2
Spherical tank	4	2
Ellipsoidal tank	$8/2.25$	$3/2$

Table 1: Dimensions of the three shapes of fuel tanks

5.2 Results

The following figures represent the sloshing behaviour and forces acting on the spacecraft where water is used as the liquid in the fuel tank. The deceleration and rotation are identical for all three simulations and the forces acting on the spacecraft follow the calculations presented before. Deceleration pushing the liquid to the right and gravitation pulling the liquid downwards into initial position. The spacecraft turns 90 degrees and thus at $t = 35$ the cylindrical spacecraft (with tank inside) stands upright with the liquid still pulled to the bottom by the gravitational force.

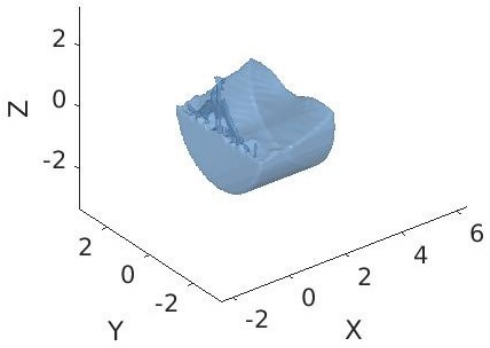

(a) t = 5.5s

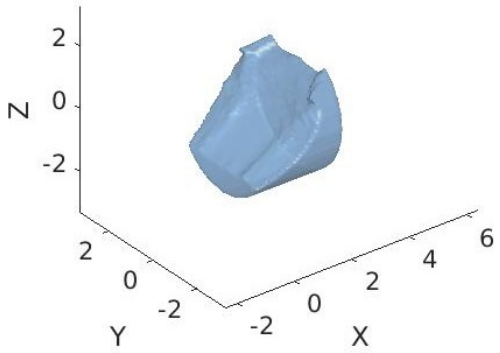

(b) t = 12.5s

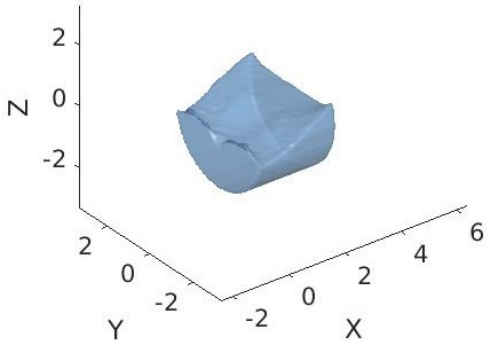

(c) t = 20s

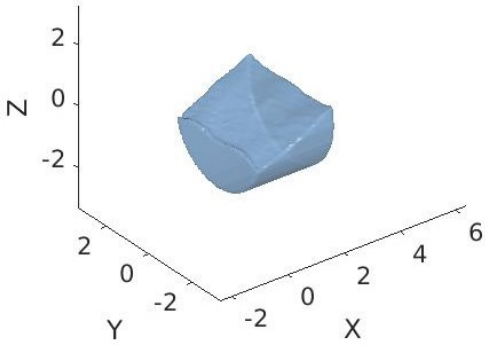

(d) t = 25s

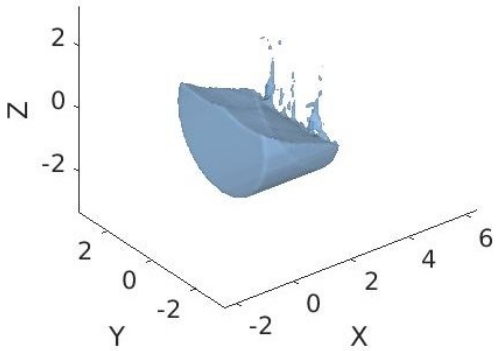

(e) t = 30s

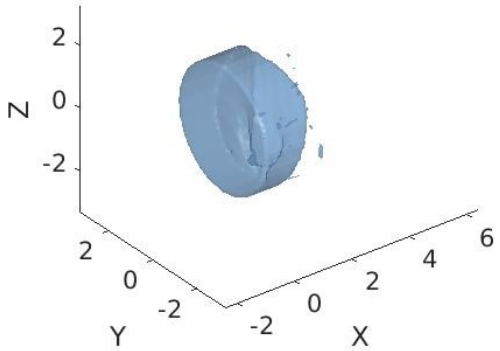

(f) t = 35s

Figure 7: Snapshots of the cylinder simulation

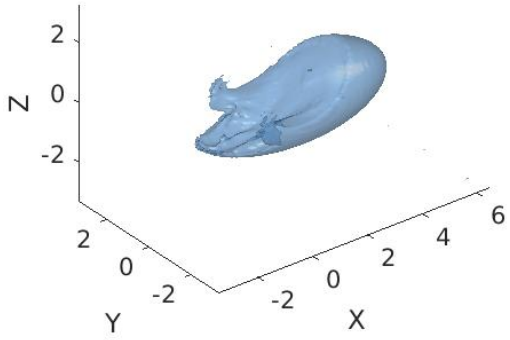

(a) t = 5.5s

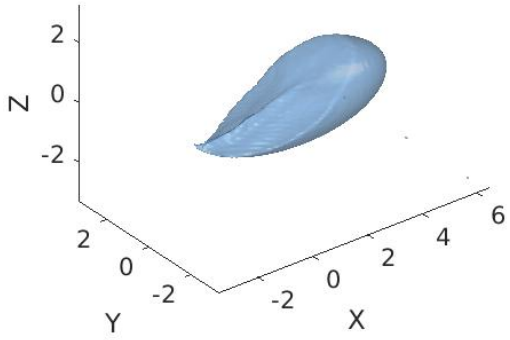

(b) t = 12.5s

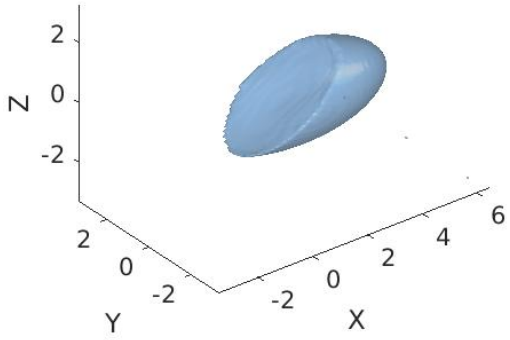

(c) t = 20s

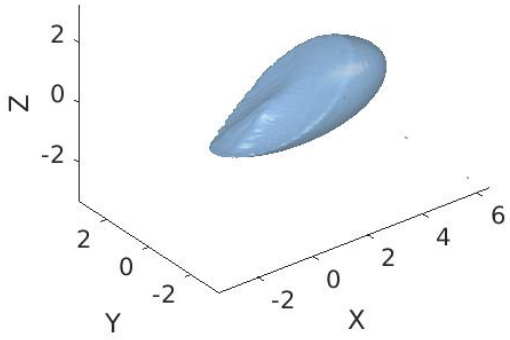

(d) t = 25s

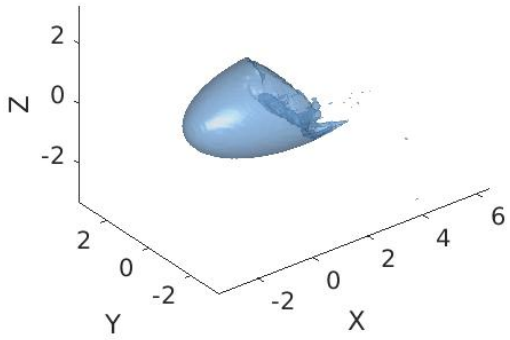

(e) t = 30s

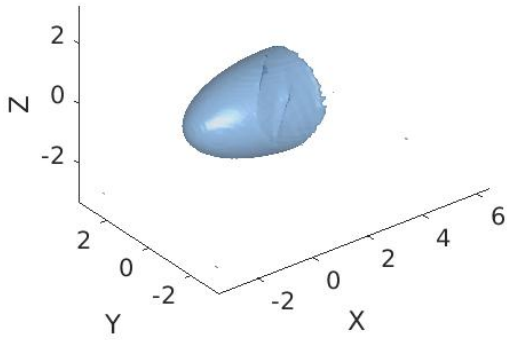

(f) t = 35s

Figure 8: Snapshots of the ellipsoid simulation

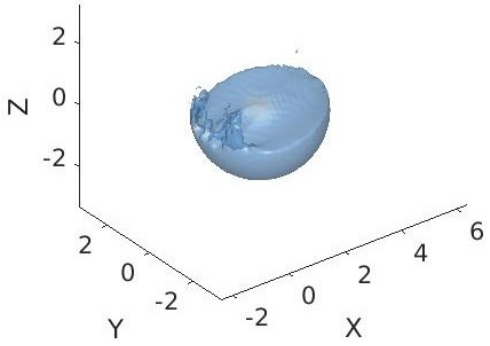

(a) t = 5.5s

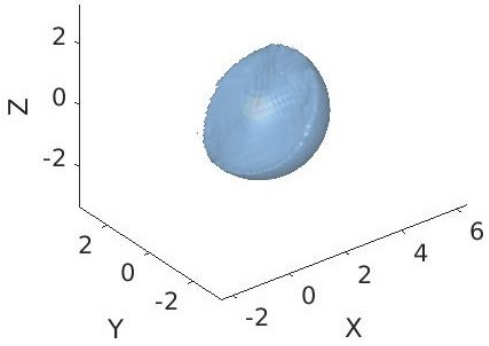

(b) t = 12.5s

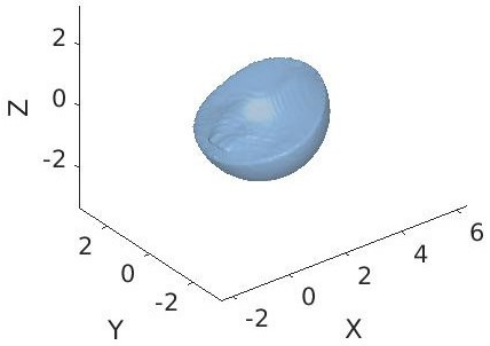

(c) t = 20s

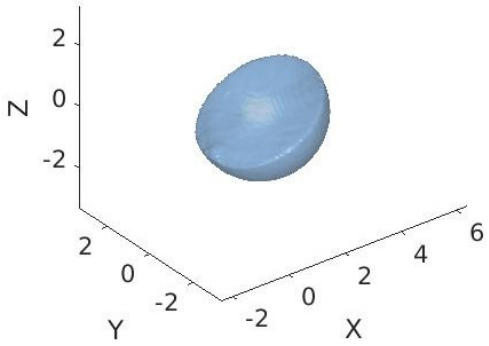

(d) t = 25s

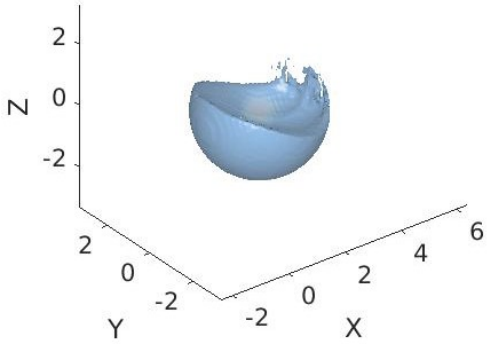

(e) t = 30s

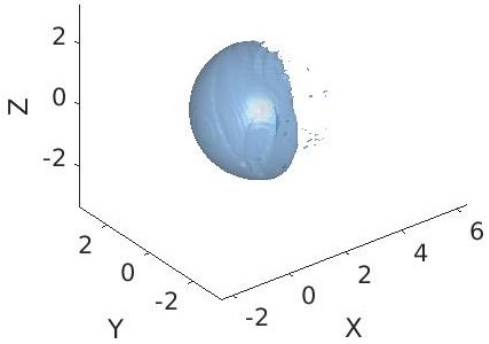

(f) t = 35s

Figure 9: Snapshots of the sphere simulation

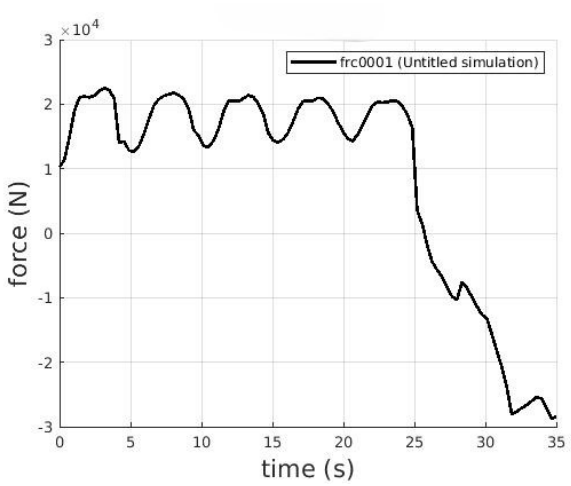

(a) X Forces Cylinder

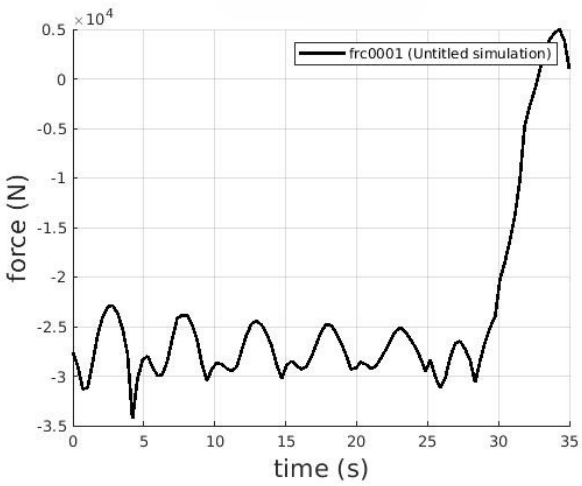

(b) Z Forces Cylinder

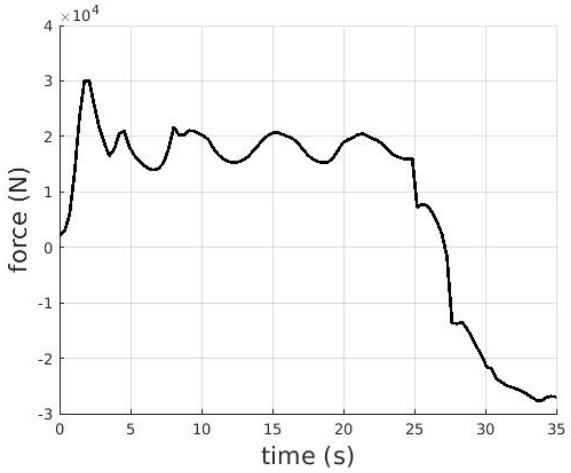

(c) X Forces Ellipsoid

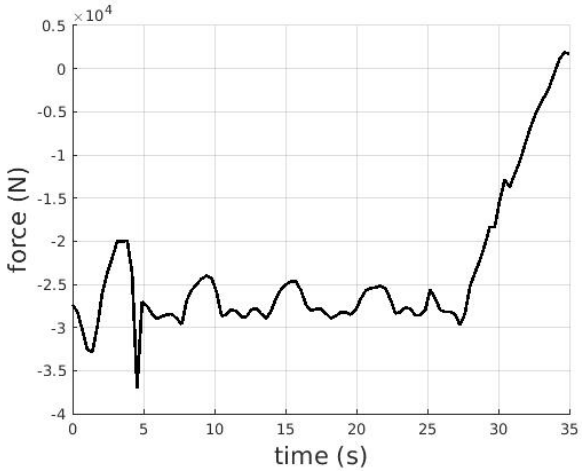

(d) Z Forces Ellipsoid

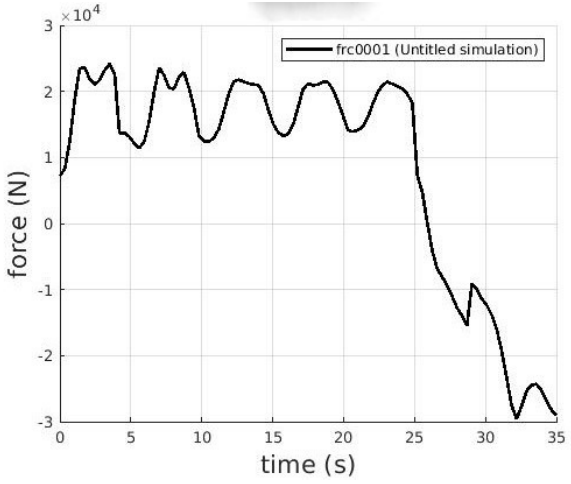

(e) X Forces Sphere

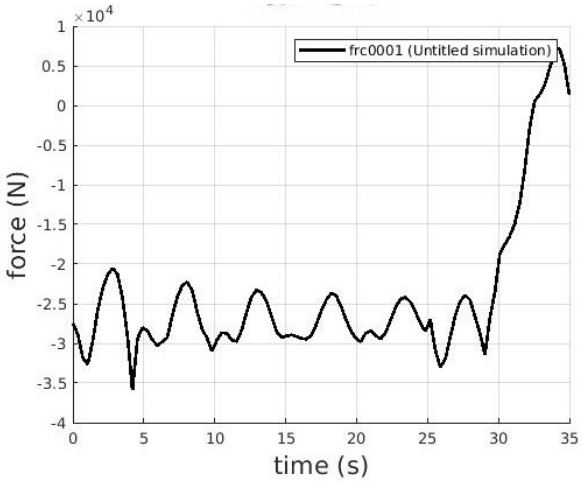

(f) Z Forces Sphere

Figure 10: Forces on the fuel tank of different shape

5.3 Observations

Three simulations were done to compare the effect of different shapes of fuel tanks in spaceships trying to perform a landing manoeuvre on the moon. As shown in the figures in the previous section, these three simulations were done with the same ComFLOW parameters except the different shapes of the fuel tank and consequently also different shapes of body of fluid.

From the force graphs portrayed in Figure 10 it is not clear that a smoother surface reduces the peak force of the liquid applied to the fuel tank for this specific manoeuvre. The spherical tank displays similar forces in both the x- and z orientation and even has slightly higher peaks. The values for the force in the direction of the x-axis are indeed fluctuating around the calculated value of $F_x = 1.8 * 10^4 N$ during the deceleration for all three fuel tanks. These fluctuations can be largely credited to the sloshing inside the tank. Even though the total forces are very alike, there is a noteworthy difference in the snapshots displayed in Figures 7 and 9, where less extreme water splash peaks are observed at most time frames.

Considering the ellipsoid case, there is an interesting benefit visible in Figures 10c and 10d. The fluid configuration shows less volatile graphs compared to the cylindrical and even the spherical case. Though the ellipsoidal tank experiences a large peak in force in the beginning of the deceleration process, both forces in z- and x- direction are 'smoother' than the two other cases suggesting less powerful propellant slosh. In Figure 8 this result is further visualized and indeed less slosh is observed throughout the manoeuvre with the exception of the first part of the deceleration.

As stated before, the volume of the tank stayed the same throughout the simulations, because the same volume and weight of fuel is important in this scenario. This means however that the length (x-axis) is significantly larger in the spherical setup. Changing the shape of the fuel container and therefore maybe changing the shape of the entire spacecraft is not without consequences. As explained earlier, to be able to simulate with the same amount of fuel while still having a 50 % filled container, the sphere needed to be larger in the x- and y- direction. The ellipsoidal tank is not wider but instead longer, which produces the same problem in the fact that increasing the size of a rocket drastically impacts the aerodynamics and fuel needed to complete the journey. This notion might make this solution to reduce the effects of sloshing "not worth it", but this will have to be investigated more.

Note that the frame of the simulations is attached to the fuel tank. I.e. at $t = 30s$ the spacecraft and fuel tank have rotated 45 degrees but in the snapshots they still appear in the horizontal position because of this fixed frame. This notion is important to keep in mind when observing the liquid configuration in snapshots that are under rotation. The liquid being in the bottom right corner at $t = 30s$ is logical when taking this into account. In section 7 this concept will be critical for understanding the force graphs.

6 Effect of Fuel Type on Propellant Slosh

The simulations in the previous section were done using water as the fluid in the three differently shaped fuel tanks. Denser fluids have higher inertia and thus tend to exhibit more pronounced sloshing behavior and yield higher forces. Different agencies have used different types of fuel in the past and therefore this section tries to analyze and demonstrate the major differences in the propellant slosh generated by changing the liquid in the fuel tank. Three fuel types that are most prominently used throughout the last decades are different kinds of ethanol (EtOH), refined kerosene (RP-1) and liquid hydrogen (LH2) [7],[8]. The sloshing phenomenon is influenced by the inertia of the fluid, which is determined by its density. Therefore, denser fuels, such as RP-1, are more prone to sloshing compared to less dense fuels like liquid hydrogen. Next to the forces in the X and Z direction, also snapshots are displayed to visually grasp the differences in slosh levels again. For the comparison with water, note that the force graphs and snapshots of this section can be compared with Figures 7, 10a and 10b in Section 5.

6.1 Parameters

Most of the ComFLOW parameters used in the upcoming simulations are similar to the cylinder filled 50% with water and as such the parameters describing the geometry and the initial liquid configuration are identical to that simulation. The cylinder with water is used here again as comparison but snapshots of that simulation will not be repeated as they are portrayed in Section 5. The changed parameters are density ρ, dynamic viscosity μ and surface tension σ. The values in Table 2 are for a chosen temperature of 20° Celsius (or 293 Kelvin). This agrees with the controlled temperature of most internal fuel tanks in space, which lies between 280K and 330K approximately.[9] The force calculated similarly as in equations 7 and 8 is also displayed in Table 2.

	$\rho(kg/m^3)$	$\mu(Pa*s)$	$\sigma(N/m)$	$F_x(N)$	$F_z(N)$
Water	$1*10^3$	$1*10^{-3}$	$7.3*10^{-2}$	$1.8*10^4$	$-2.7*10^4$
EtOH	789	$1.2*10^{-3}$	$2.2*10^{-2}$	$1.4*10^4$	$-2.1*10^4$
RP-1	810	$3.3*10^{-3}$	$2.7*10^{-2}$	$1.5*10^4$	$-2.2*10^4$
LH2	70.85	$1.14*10^{-5}$	$1.86*10^{-3}$	$1.3*10^3$	$-1.9*10^3$

Table 2: Fuel properties (20° Celsius) [10][8]

6.2 Results

The following figures represent the sloshing behaviour and forces acting on the spacecraft where the three fuel types, ethanol, RP-1 and LH2 are used as the liquid in the fuel tank. The deceleration and rotation are identical and a cylindrical fuel tank is used for all three simulations.

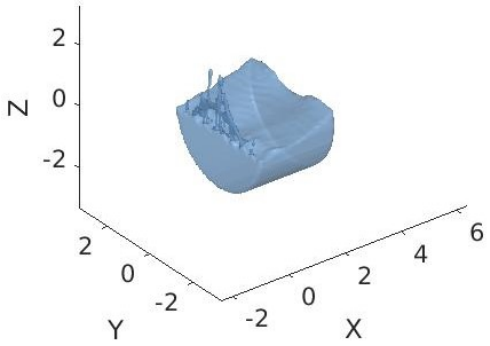

(a) t = 5.5s

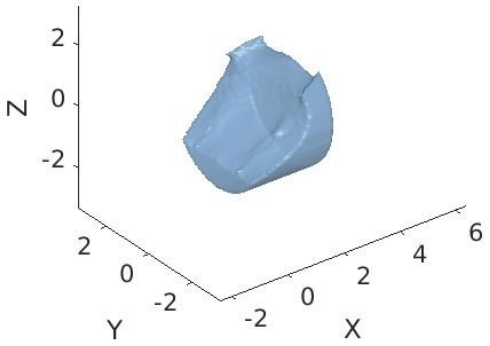

(b) t = 12.5s

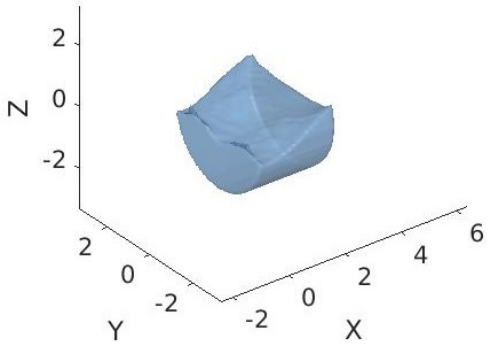

(c) t = 20s

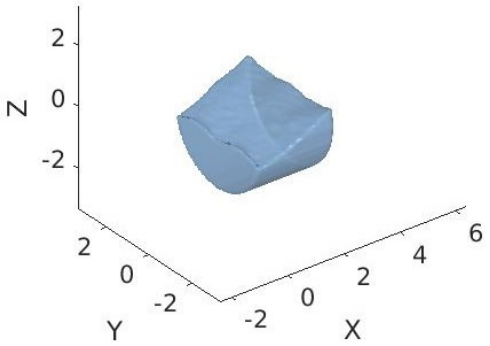

(d) t = 25s

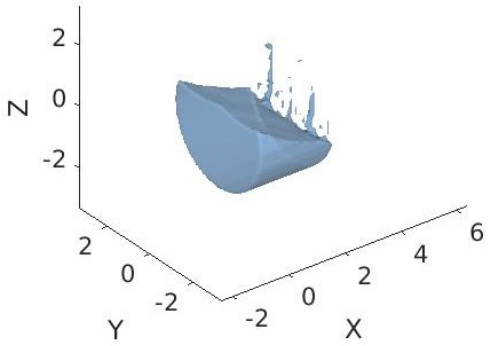

(e) t = 30s

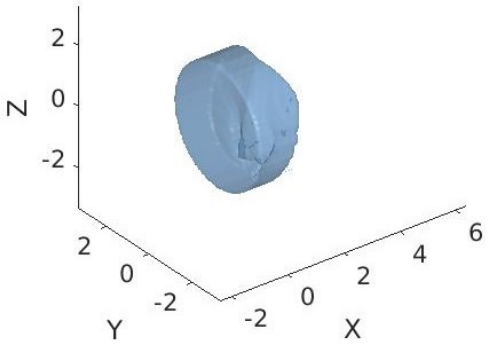

(f) t = 35s

Figure 11: Snapshots of the Ethanol simulation

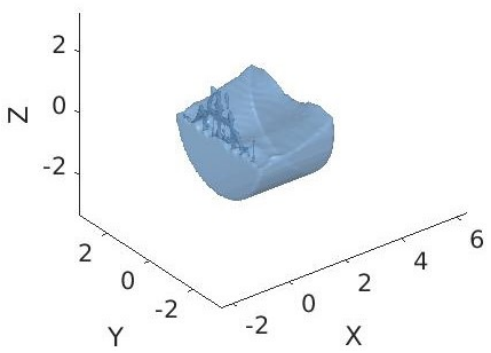

(a) t = 5.5s

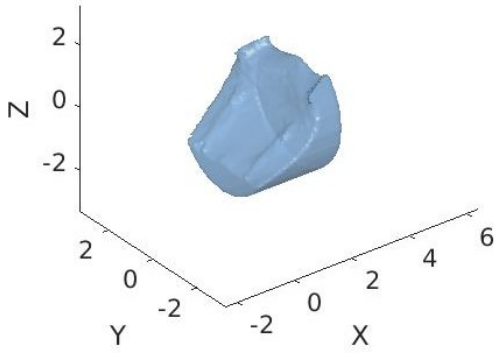

(b) t = 12.5s

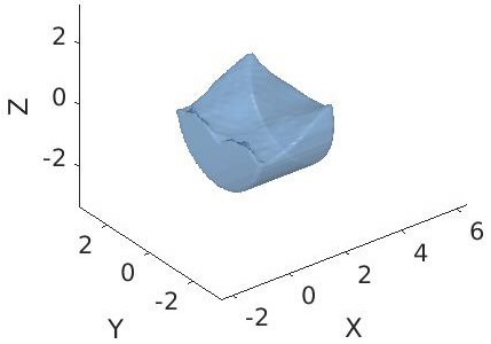

(c) t = 20s

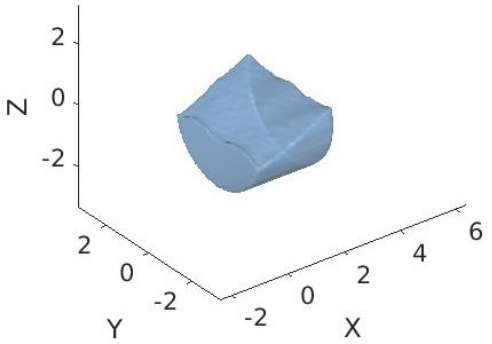

(d) t = 25s

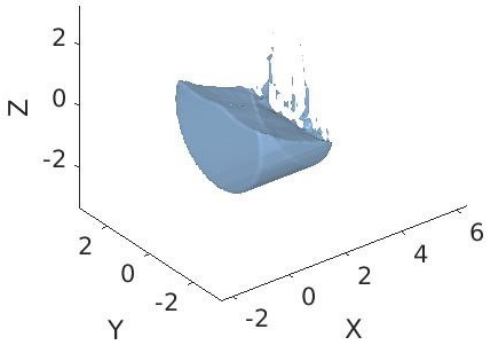

(e) t = 30s

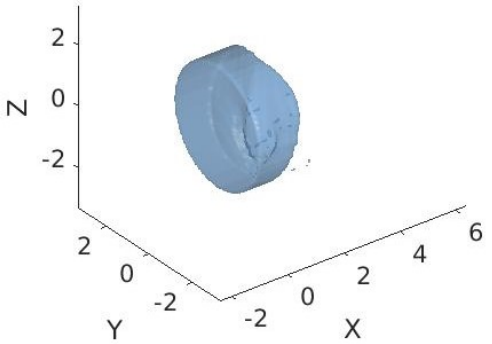

(f) t = 35s

Figure 12: Snapshots of the RP-1 simulation

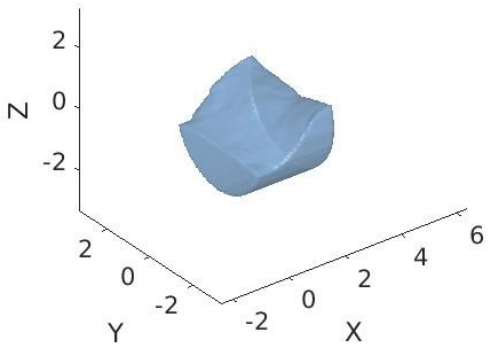

(a) t = 5.5s

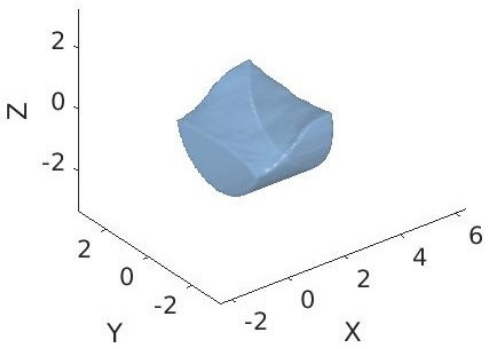

(b) t = 12.5s

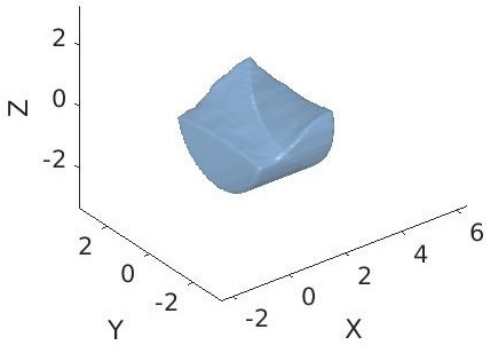

(c) t = 20s

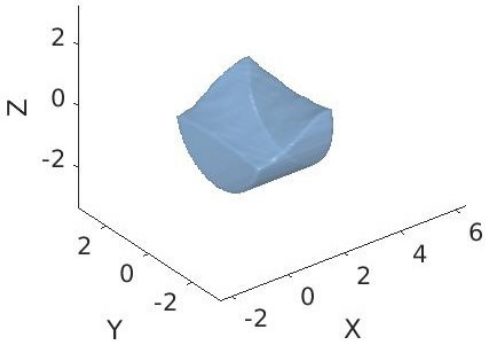

(d) t = 25s

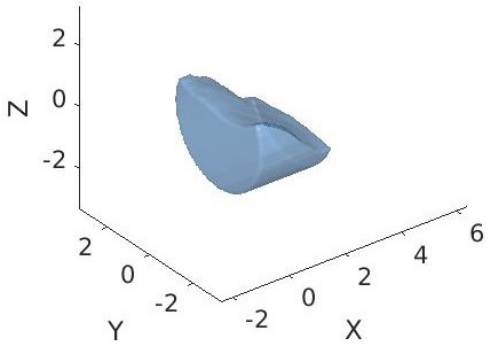

(e) t = 30s

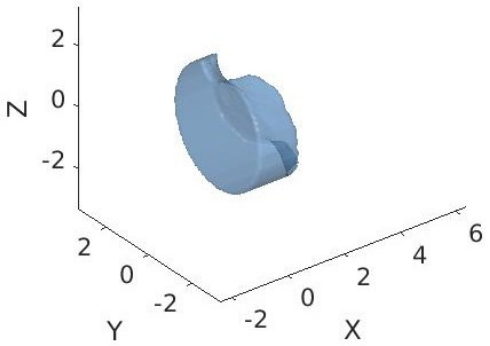

(f) t = 35s

Figure 13: Snapshots of the liquid hydrogen simulation

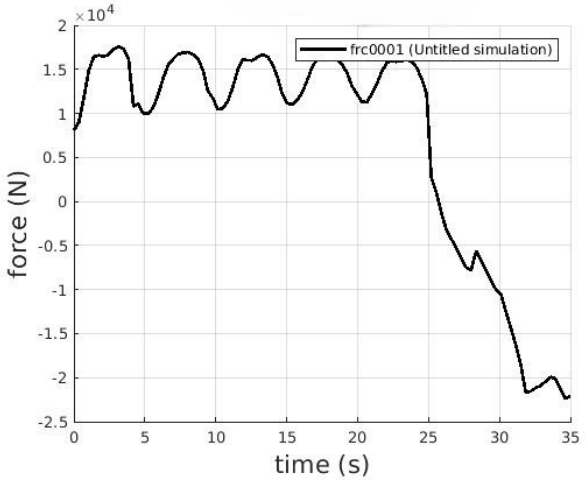

(a) X Forces Ethanol

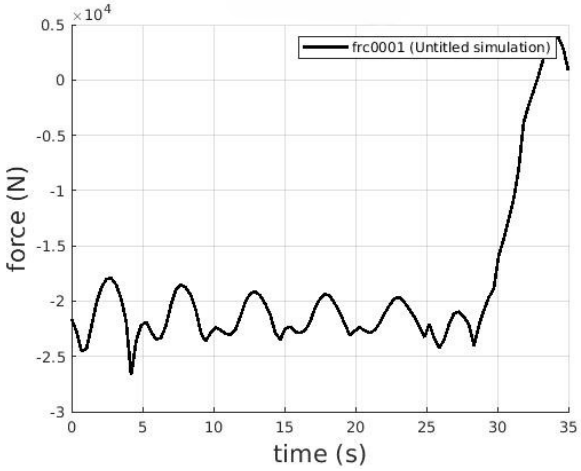

(b) Z Forces Ethanol

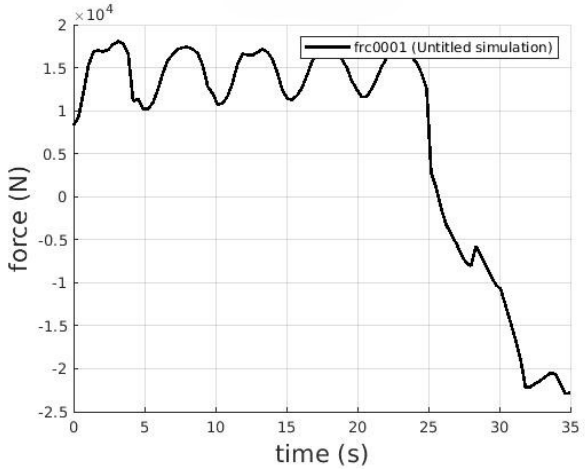

(c) X Forces RP-1

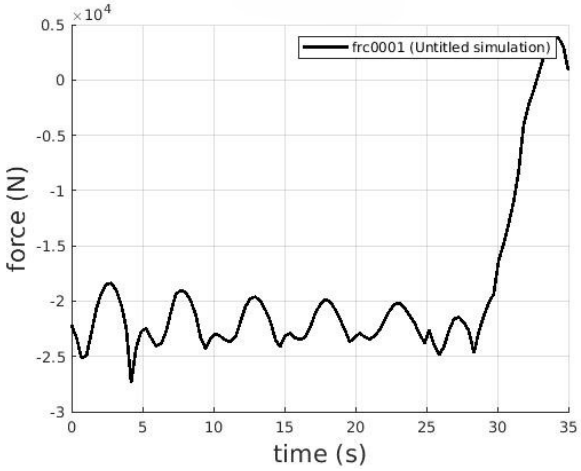

(d) Z Forces RP-1

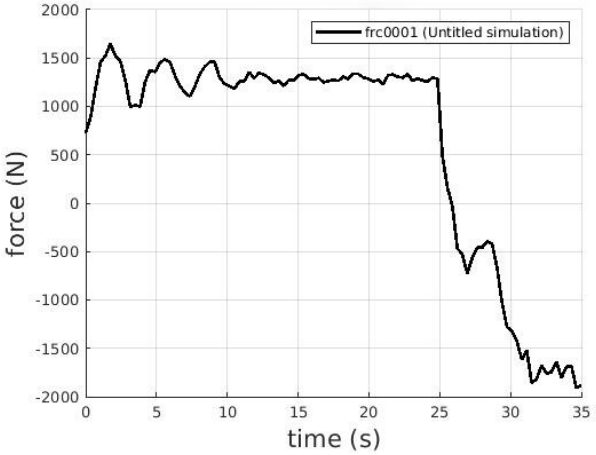

(e) X Forces Liquid Hydrogen

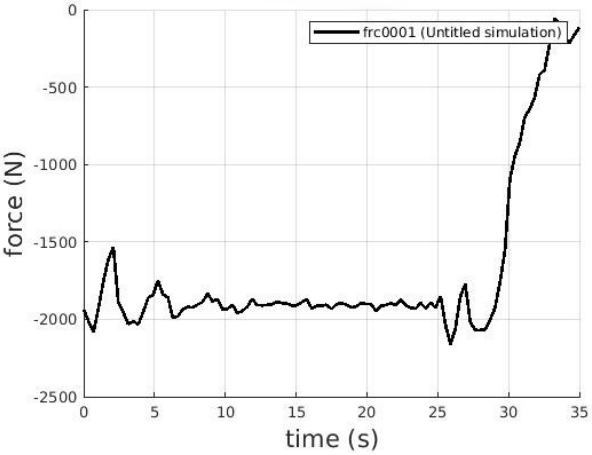

(f) Z Forces Liquid Hydrogen

Figure 14: Forces on fuel tank of different fuel types

6.3 Observations

In the graphs of Figure 14 the force effects are displayed, obtained for the entire body of the simulation during a 35 second landing procedure. Figures 11 to 13 show the state of the liquid at certain times during the simulation.

First note that the total force graphs in the Z-axis are mainly generated by the gravity of the moon and therefore the forces portrayed in the graphs oscillate around this dominant gravitational force. The difference between the extreme values and the calculated gravitational force in Table 2 is the force attributed to liquid sloshing. As shown in Figures 14b and 14d the forces acting on the Z - axis during these simulations are relatively similar for RP-1 and EtOH as is expected due to their similar densities and no other major changes in the calculation of the gravitational force. A more sizeable difference in force is noticeable when comparing the graph of liquid hydrogen. As its density is much lower than the other three liquids (including water), the average but also peak force is significantly less, comparing a peak force of almost $F_{Z,Water} = -3.5 * 10^4 N$ during the water simulation with $F_{Z,LH2} = -2.2 * 10^3 N$ for the current simulation.

Now consider the total forces acting on the X axis of the fuel tank. The force exhibits similar behaviour in forming a wave pattern, eventually vanishing when the deceleration ends. The interaction of the gravitational force with the deceleration force of the spacecraft results in similar observations as about the z - axis. A lower density liquid seems to impact the force acting on the moving body. From the peak values for the different fuel types similar differences are observable. Figure 14e again shows the effect density has on the sloshing behaviour. During the initial part of the deceleration the peaks of the wave are at a maximum of $F_z = 0.5 * 10^3 N$ away from the deceleration force, which is a factor 10 lower. As with Section 5 researching different shapes, in this section three simulations were done doing the horizontal landing. The perceptible result is that a lower density liquid causes less force on the spacecraft in both z- and x-axis direction and therefore less slosh. The highest force peak recorded during these simulations is associated with the water filled tank which has the highest density liquid.

A small note is that EtOH, RP-1 and LH2 are different in the way they produce energy and this means that different ignition and storage systems are needed to start movement. A LH2 spacecraft needs an LOX (liquid oxygen) tank as well for the process of energy creation [11]. As a consequence the total slosh difference with the other two fuel types might be less impressive than stated in this section.

7 Changing the landing manoeuvre

The manoeuvre initially constructed is such that rotation happens while moving with minimal velocity, which is the most intuitive approach to the process of aligning with the moon with minimal propellant slosh. A different approach, however, might make a difference in the sloshing effects over the course of the activity. In the original manoeuvre the rotational movement is made near the end of the entire procedure and as such near the time of landing. It could be beneficial to rotate earlier in the total manoeuvre to reduce sloshing near the landing moment. To this end, two new simulations are done, comparing once again to the starting setup explained in Section 4. The fuel tank is again chosen to be cylindrical for this, and the fuel type stays water. To get significant results, the total time it takes for all manoeuvres stays 35 seconds.

The first simulation for which the results are shown below is done by reversing the order in which the deceleration and turning process happen. While conserving a constant speed of 27.8 m/s, the spacecraft will first turn the necessary 90 degrees to align its landing gear with the moon. This procedure will happen over the 10 seconds from t_A to t_B from Figure 4. Afterwards, while already in the correct position, the spacecraft decelerates to a velocity of 1 m/s over the next 25 seconds from t_B to t_D.

The second additional manoeuvre looked at in this section is the operation where deceleration and turning happen simultaneously. The spacecraft will perform both the rotation as well as decelerate during the first 25 seconds. This means the rotation takes 2.5 times as long as in the original manoeuvre, which is expected to reduce the sloshing caused by this rotation. The rotational displacement, velocity and acceleration change according to

$$\omega(t) = \begin{cases} -\frac{\alpha(t^2)}{2}, & t \in [0, 12.5] \\ -(25 * \alpha * (t) - \frac{\alpha(t)^2}{2} - \frac{\pi}{2}), & t \in [12.5, 25] \end{cases} \tag{9a}$$

$$\dot{\omega}(t) = \begin{cases} -\alpha * (t), & t \in [0, 12.5] \\ -(25\alpha - (t)\alpha), & t \in [12.5, 25] \end{cases} \tag{9b}$$

$$\ddot{\omega}(t) = \begin{cases} -\alpha, & t \in [0, 12.5] \\ \alpha, & t \in [12.5, 25] \end{cases} \tag{9c}$$

where $\alpha = \frac{\pi}{2(\frac{t_C - T_A}{2})^2} = \frac{\pi}{625}$.

During the last 10 seconds of the procedure, no deceleration or rotation happens and it continues with a constant speed of 1m/s while already having aligned the bottom of the spacecraft with the surface of the moon. This could give the spacecraft room in the last part ($t \in [t_C, t_D]$) of the journey, to correct for any sloshing effects that could have occurred during the first part of the process.

7.1 Results

The following snapshots and force graphs display the behaviour of liquid in a fuel tank performing the previously described manoeuvre. To compare to the original half filled fuel tank carrying out the original manoeuvre the fuel tank is kept cylindrical again and water was used as liquid inside the tank.

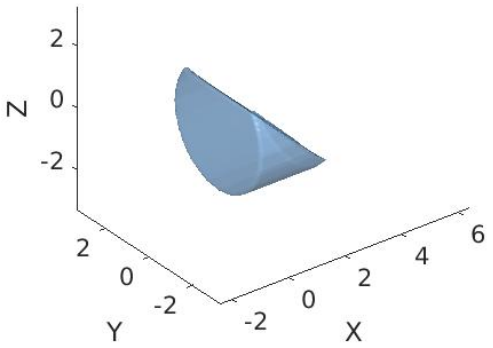

(a) t = 5.5s

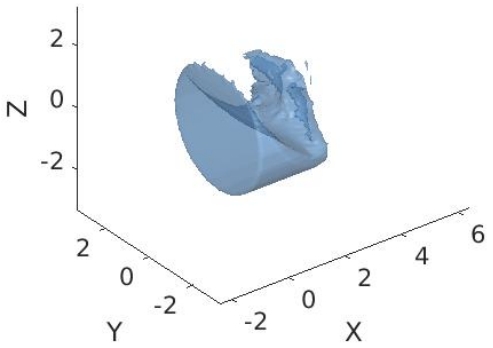

(b) t = 12.5s

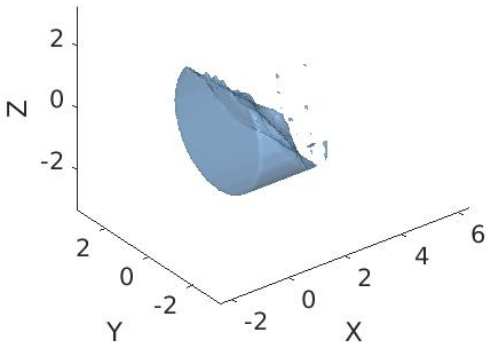

(c) t = 20s

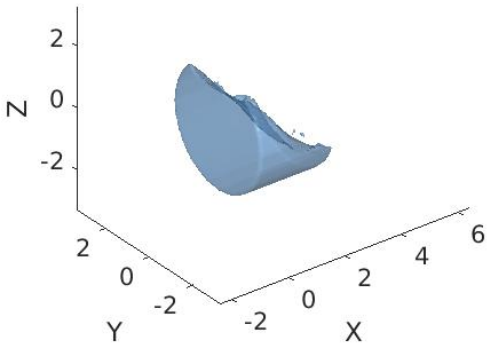

(d) t = 25s

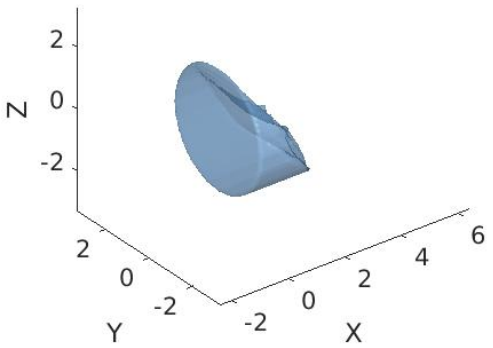

(e) t = 30s

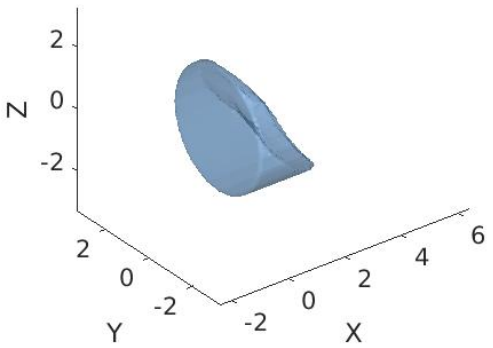

(f) t = 35s

Figure 15: Snapshots of the rotation first simulation

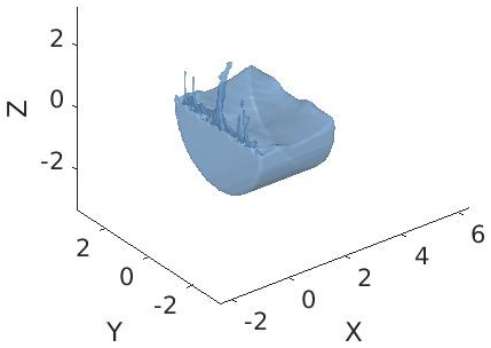

(a) t = 5.5s

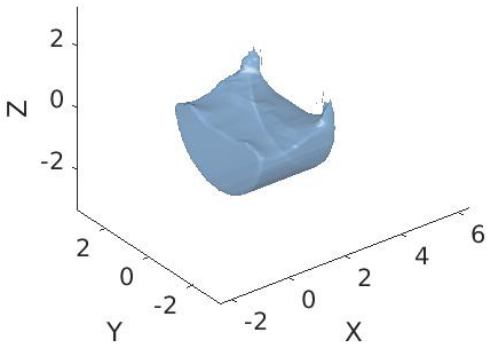

(b) t = 12.5s

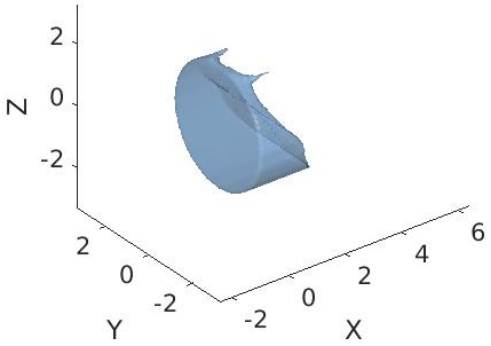

(c) t = 20s

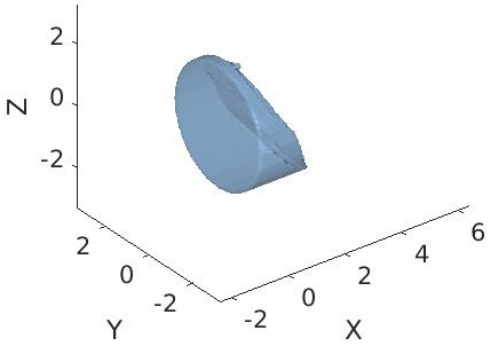

(d) t = 25s

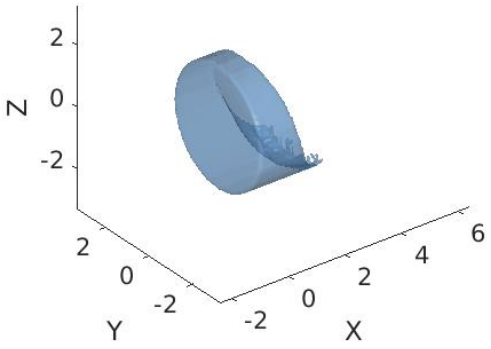

(e) t = 30s

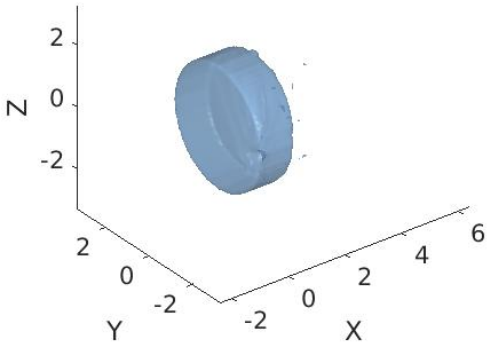

(f) t = 35s

Figure 16: Snapshots of the simultaneous rotation and deceleration simulation

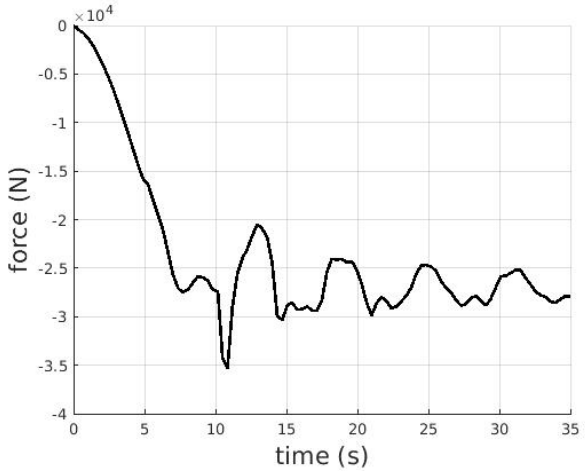

(a) X Forces rotation first

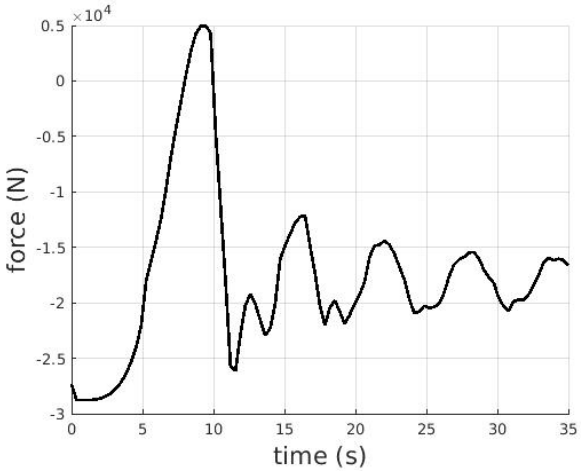

(b) Z Forces rotation first

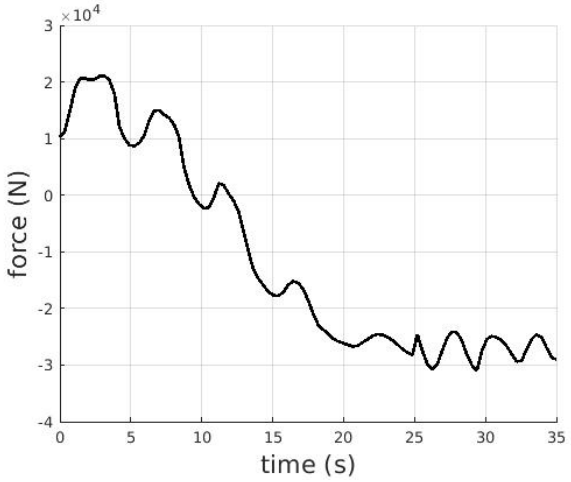

(c) X Forces simultaneous

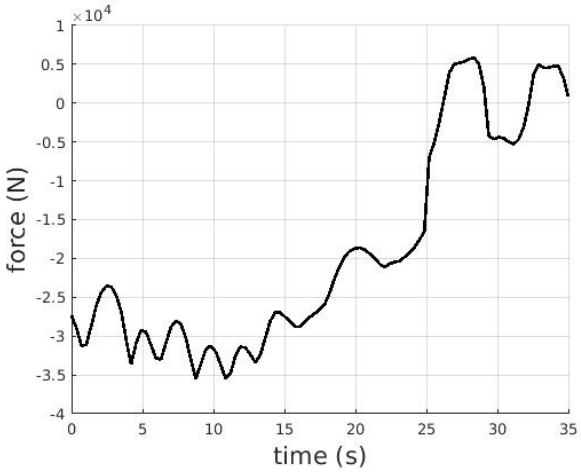

(d) Z Forces simultaneous

Figure 17: Forces for different manoeuvres

7.2 Observations

When observing the force graphs in simulations where rotation is happening from the beginning, the frame attached to the fuel tank comes into play again. The forces for deceleration are working in the direction of the x-axis of the fuel container. The fuel tank rotates while being attached to the frame such that the deceleration forces end up working in the direction of the z-axis according to the force box. Note that this is indeed the case as in the force graph of 17b the wave after rotation oscillates around $-1.8 * 10^4 N$ which agrees with the deceleration force. From the reference frame of for example the moon or an outside observer this force would still be in the direction of the x-axis.

First note the force graph in the horizontal (x) direction of the simulation, where rotation happens before deceleration. This graph shows behaviour similar to the original manoeuvre during the deceleration process. The wave oscillates with peaks reaching almost $F_x = 1 * 10^4 N$ from the equilibrium at the start of the deceleration (thus immediately after finishing the rotation), which is reason to believe that the rotation at full speed results in an increase of slosh at this point. Near the end of the manoeuvre, however, the peaks reduce to similar heights of approximately $F_x = 0.5 * 10^4 N$ concurring with the end of deceleration in the original manoeuvre. The forces in the z direction portrayed in the Figure 17b agree with the previous statement. This graph displays divergence from the gravitational force starting at a difference of $F_z = 1.35 * 10^4 N$ and dampens out to $F_z = 0.5N * 10^4$. This last value agrees with the original manoeuvre, but the forces during the rotation at full speed and the start of the deceleration process exhibit an increase in slosh and therefore this manoeuvre seems unlikely to improve the reliability of the landing procedure. From the snapshots in Figure 15 this is confirmed. Especially Figure 15b at $t = 12.5s$, after rotating and starting to decelerate for $2.5s$ a relatively large amount of slosh is observed with the fuel 'slamming' into the rotated front of the fuel tank. The snapshots display similar behaviour of slosh during the rest of the manoeuvre. As stated before regarding the simultaneous manoeuvre, even though the average amount of slosh is increased, the largest effects of slosh are in the first half of the procedure. This gives rise to the idea that it might be beneficial to experience this slosh early and not close to the landing moment. The methods in space travel that correct for forces on the spacecraft caused by propellant slosh are beyond the scope of this research.

The manoeuvre where rotation and deceleration both happen during the first 25 seconds ($t_A - t_C$) also leads to interesting results. From the snapshots in Figure 16 there is no clear difference in slosh compared to the original manoeuvre. Looking at the forces in Figures 17c and 17d, this is partly confirmed by the peaks during the first 25 seconds, which are less high than the original manoeuvre but still stay around $F_x = 0.5 * 10^4 N$ in the last 10 seconds. This suggests that the 10 seconds in $t_C - t_D$ will not be enough to correct for any sloshing since slosh is still dampening out during this time frame. Overall this manoeuvre does seem to decrease the effects of slosh on the spacecraft, especially the effects caused by rotation, which is largely amounted to the fact that the rotation is over a time frame that is 2.5 times as large as the original.

In the last 15 seconds of graph 17d something strange happens, where a wave-like force signal with large amplitude occurs. During this time the spacecraft undergoes neither rotation nor deceleration and thus sloshing effects are expected to be minimal. What is happening exactly is not deciphered and might be interesting to be explored in further research.

8 Conclusion

This research has provided insights into the complex dynamics of propellant slosh during moon landing manoeuvres, considering various factors such as the shape of the fuel tank, different fuel types, and different manoeuvres. Through simulation and analysis, several key findings have emerged.

Firstly, the shape of the fuel tank has a significant impact on propellant slosh behavior. Tanks with non-conventional shapes, such as ellipsoidal designs, exhibit different slosh characteristics compared to traditional cylindrical tanks. Though the difference between a spherical and cylindrical tank were negligible, the ellipsoidal tank displayed reduced force caused by propellant slosh. Note that changing the shape of a spacecraft has more complicated repercussions than only reducing propellant slosh. Understanding how these variations affect slosh dynamics is essential for optimizing spacecraft design and performance.

Furthermore, lower density liquids, such as liquid hydrogen (LH2), result in lower average and peak forces compared to denser fluids like water, RP-1, and EtOH. These findings suggest that the choice of fuel type plays a crucial role in determining the magnitude of slosh-induced forces experienced by the spacecraft during landing manoeuvres. Specifically, lower density fuels exhibit reduced sloshing effects, leading to lower peak forces on the spacecraft. The implications of these findings extend to the design and engineering considerations for spacecraft fuel systems. While the differences in sloshing behavior between fuel types are existent, factors such as the energy production process and associated storage systems may influence the overall impact on spacecraft dynamics.

Finally, the analysis of two different landing manoeuvres was done, one where rotation precedes deceleration and another where rotation and deceleration occur simultaneously, but with prolonged rotation operation. This sheds light on their impacts on sloshing behavior during the landing procedure. For the maneuver where rotation happens before deceleration, significant sloshing effects are observed, particularly at the beginning of the deceleration phase. This is attributed to the slosh induced by the preceding rotation, resulting in similar or higher peaks in force oscillations in both the X and Z axes compared to the original manoeuvre. However, as the deceleration progresses, these peaks gradually become lower, indicating a dampening of sloshing effects. Ultimately, this manoeuvre appears unlikely to improve the reliability of the landing procedure due to the heightened sloshing during the initial phase.

Contrarily, in the manoeuvre where rotation and deceleration occur simultaneously, sloshing effects are reduced. The extended duration of rotation allows for a smoother transition of the fluid, even though deceleration happens at the same time, resulting in lower peak forces and dampened sloshing behavior throughout the maneuver. Despite a slight increase in average sloshing, the overall impact on spacecraft stability is mitigated due to the more controlled sloshing dynamics. While both manoeuvres offer insights into sloshing behavior, the simultaneous rotation and deceleration shows promise in minimizing slosh-induced disturbances, particularly during critical phases of the landing procedure. Further research of this approach could lead to improvements in spacecraft stability.

8.1 Discussion

Though this research provided some noteworthy results, a few remarks have to be made.

Important research still needs to be done to further identify the impact of propellant slosh and ways to minimize it. In this research, the forces on the spacecraft were not allowed to move the spacecraft, but instead the spacecraft was locked into position. In real world scenarios, like Apollo 11, the sloshing of fuel can greatly impact the global movement of the spacecraft. This can lead to wobbling or swaying completely out of course. Interesting future research therefore is the modeling of a spacecraft with fuel tank that actually feels the impact of the propellant slosh and moves if the force this slosh produces is large enough.

The analysis of different landing maneuvers highlights the potential impact of spacecraft motion on slosh behavior. Future research could explore alternative landing techniques, such as hovering or controlled descent, to further minimize slosh-induced disturbances during critical phases. Additionally, investigating the use of autonomous landing systems that optimize spacecraft trajectories to reduce slosh effects could improve overall mission efficiency.

Improving the accuracy of computational models for predicting slosh behavior is essential for optimizing spacecraft design and mission planning. Future research could focus on refining these models through expanding the grid or using higher accuracy discretization. Additionally, experimental validation of simulation results in relevant lunar environments, such as microgravity test facilities or lunar analog sites, would be valuable for confirming the effectiveness of slosh mitigation strategies.

Through extensive research over the past decades space exploration has become relatively easier and safer. The problems Apollo 11 encountered in 1969 will probably not be experienced in that magnitude again, but this does not necessarily mean that the problem of liquid propellant sloshing in a spacecraft is solved in general. To this day it remains a difficult consideration while preparing for a space mission. With more research to this intricate problem the final frontier will surely remain a fascinating place of exploration.

Figure 18: Apollo 11 Lunar Module Eagle in landing configuration[12]

References

[1] R. J. Gran and O. Saarela, "The apollo 11 moon landing: Spacecraft design then and now," *MathWorks*, 2019.

[2] R. D. Ashruf, "Simulations of sloshing during maneuvers in space," *University of Groningen*, 2020.

[3] R. Luppes *et al.*, "Manual comflow version 3.9.x / 4.0," *University of Groningen*, 2015.

[4] U. A. C. of Engineers, "Hec-ras hydraulic reference manual," *Hydrologic Engineering Center*, 2023.

[5] C. Hewgley and O. Yakimenko, "Precision guided airdrop for vertical replenishment of naval vessels," 05 2009.

[6] M.-A. Xue, Y. Chen, J. Zheng, L. Qian, and X. Yuan, "Fluid dynamics analysis of sloshing pressure distribution in storage vessels of different shapes," *Ocean Engineering*, vol. 192, 2019.

[7] Unknown, "What kind of fuel do rockets use and how does it give them enough power to get into space?," *Scientific American (website)*, 2006.

[8] R. A. Braeunig, "Basics of space flight: Rocket propellants," *braeunig.us*, 2008.

[9] C. L. Mosier, "Map propulsion system thermal design," *NASA GSFC*, 2001.

[10] T. Fujikawa, T. Tsuchiya, and S. Tomioka, "Multidisciplinary design optimization of a two-stage-to-orbit reusable launch vehicle with ethanol-fueled rocket-based combined cycle engines," *Transactions of the Japan society for aeronautical and space sciences*, vol. 60, no. 5, pp. 265–275, 2017.

[11] Unknown, "Innovative liquid hydrogen storage to support space launch system," *NASA website*, 2018.

[12] Unknown, "Apollo 11, the moon landing," *National Air and Space Museum*.

9 Appendix A: Grid conversion study results

In this appendix the results are displayed of the grid conversion study. The force graph and snapshot on the left correspond to the spherical fuel tank filled with water performing the original manoeuvre with a grid size of 80x80x80. The force graph and snapshot on the right correspond to the simulation using same manoeuvre and fuel tank but with a grid of 120x120x120.

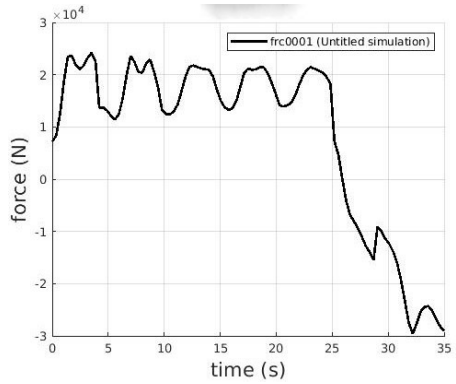

(a) X Forces Coarse Grid

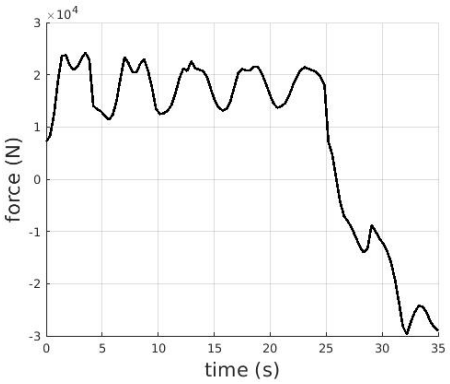

(b) X Forces Fine Grid

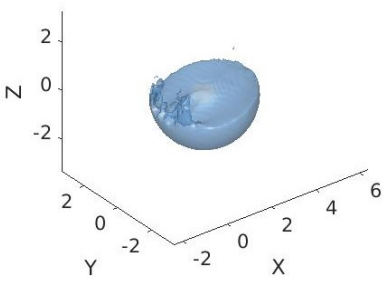

(c) Sphere t=5.5s Coarse Grid

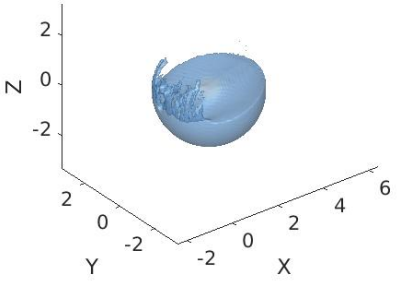

(d) Sphere t=5.5s Fine Grid

Figure 19: X Force and snapshot of coarse and fine grid simulations